The Astrophysical Journal, 891:135 (15pp), 2020 March 10 https://doi.org/10.3847/1538-4357/ab76c0

The ALMA Spectroscopic Survey in the HUDF: A Model to Explain Observed 1.1 and 0.85 mm Dust Continuum Number Counts

Gergö Popping[1,2], Fabian Walter[2,3], Peter Behroozi[4], Jorge González-López[5,6], Christopher C. Hayward[7], Rachel S. Somerville[7,8], Paul van der Werf[9], Manuel Aravena[5], Roberto J. Assef[5], Leindert Boogaard[9], Franz E. Bauer[10,11,12], Paulo C. Cortes[13,14], Pierre Cox[15], Tanio Díaz-Santos[16], Roberto Decarli[17], Maximilien Franco[18,19], Rob Ivison[1,20], Dominik Riechers[2,21,23], Hans-Walter Rix[2], and Axel Weiss[22]

[1] European Southern Observatory, Karl-Schwarzschild-Strasse 2, D-85748, Garching, Germany; gpopping@eso.org
[2] Max Planck Institute für Astronomie, Königstuhl 17, D-69117 Heidelberg, Germany
[3] National Radio Astronomy Observatory, Pete V. Domenici Array Science Center, P.O. Box O, Socorro, NM 87801, USA
[4] Department of Astronomy and Steward Observatory, University of Arizona, Tucson, AZ 85721, USA
[5] Núcleo de Astronomía de la Facultad de Ingeniería y Ciencias, Universidad Diego Portales, Av. Ejército Libertador 441, Santiago, Chile
[6] Instituto de Astrofísica, Facultad de Física, Pontificia Universidad Católica de Chile, Av. Vicuña Mackenna 4860, 782-0436 Macul, Santiago, Chile
[7] Center for Computational Astrophysics, Flatiron Institute, 162 5th Avenue, New York, NY 10010, USA
[8] Department of Physics and Astronomy, Rutgers, The State University of New Jersey, 136 Frelinghuysen Road, Piscataway, NJ 08854, USA
[9] Leiden Observatory, Leiden University, P.O. Box 9513, NL-2300 RA Leiden, The Netherlands
[10] Instituto de Astrofísica and Centro de Astroingeniería, Facultad de Física, Pontificia Universidad Católica de Chile, Casilla 306, Santiago 22, Chile
[11] Millennium Institute of Astrophysics (MAS), Nuncio Monseñor Sótero Sanz 100, Providencia, Santiago, Chile
[12] Space Science Institute, 4750 Walnut Street, Suite 205, Boulder, CO 80301, USA
[13] Joint ALMA Observatory—ESO, Av. Alonso de Córdova, 3104, Santiago, Chile
[14] National Radio Astronomy Observatory, 520 Edgemont Road, Charlottesville, VA 22903, USA
[15] Institut d'astrophysique de Paris, Sorbonne Université, CNRS, UMR 7095, 98 bis bd Arago, F-7014 Paris, France
[16] Núcleo de Astronomía, Facultad de Ingeniería, Universidad Diego Portales, Av. Ejército 441, Santiago, Chile
[17] INAF—Osservatorio di Astrofisica e Scienza dello Spazio, via Gobetti 93/3, I-40129, Bologna, Italy
[18] AIM, CEA, CNRS, Université Paris-Saclay, Université Paris Diderot, Sorbonne Paris Cité, F-91191 Gif-sur-Yvette, France
[19] Centre for Astrophysics Research, University of Hertfordshire, Hatfield, AL10 9AB, UK
[20] Institute for Astronomy, University of Edinburgh, Royal Observatory, Blackford Hill, Edinburgh EH9 3HJ, UK
[21] Department of Astronomy, Cornell University, Space Sciences Building, Ithaca, NY 14853, USA
[22] Max-Planck-Institut für Radioastronomie, Auf dem Hügel 69, D-53121 Bonn, Germany
Received 2019 September 27; revised 2020 February 10; accepted 2020 February 13; published 2020 March 13

Abstract

We present a new semiempirical model for the dust continuum number counts of galaxies at 1.1 mm and 850 μm. Our approach couples an observationally motivated model for the stellar mass and star formation rate distribution of galaxies with empirical scaling relations to predict the dust continuum flux density of these galaxies. Without a need to tweak the IMF, the model reproduces the currently available observations of the 1.1 mm and 850 μm number counts, including the observed flattening in the 1.1 mm number counts below 0.3 mJy and the number counts in discrete bins of different galaxy properties. Predictions of our work include the following: (1) the galaxies that dominate the number counts at flux densities below 1 mJy (3 mJy) at 1.1 mm (850 μm) have redshifts between $z = 1$ and $z = 2$, stellar masses of $\sim 5 \times 10^{10}\ M_{\odot}$, and dust masses of $\sim 10^{8}\ M_{\odot}$; (2) the flattening in the observed 1.1 mm number counts corresponds to the knee of the 1.1 mm luminosity function. A similar flattening is predicted for the number counts at 850 μm; (3) the model reproduces the redshift distribution of current 1.1 mm detections; and (4) to efficiently detect large numbers of galaxies through their dust continuum, future surveys should scan large areas once reaching a 1.1 mm flux density of 0.1 mJy rather than integrating to fainter fluxes. Our modeling framework also suggests that the amount of information on galaxy physics that can be extracted from the 1.1 mm and 850 μm number counts is almost exhausted.

Unified Astronomy Thesaurus concepts: Galaxy evolution (594); High-redshift galaxies (734); Dust continuum emission (412); Interstellar medium (847); Galaxy formation (595)

1. Introduction

Dust-obscured star formation contributes importantly to the cosmic star formation history of our universe (see the review by Madau & Dickinson 2014). Ever since the infrared (IR) extragalactic background light (EBL) was first detected by the *Cosmic Background Explorer*, it has become clear that the IR contributes to about half of the total EBL (Puget et al. 1996; Fixsen et al. 1998). Understanding which galaxies are responsible for the IR EBL is therefore a key requirement toward understanding which galaxies contribute most actively to the dust-obscured cosmic star formation, thereby providing critical constraints for galaxy formation models (Granato et al. 2000; Baugh et al. 2005; Fontanot et al. 2009; Somerville et al. 2012; Cowley et al. 2015).

A commonly used approach to better quantify the IR EBL has been to measure the number counts of galaxies at IR wavelengths. Because of the negative *k*-correction, the preferred wavelength range to do this has been the submillimeter and millimeter regime. The first efforts to measure number counts were carried out with single-dish instruments such as SCUBA and LABOCA (Eales et al. 2000; Smail et al. 2002; Coppin et al. 2006; Knudsen et al. 2008; Weiß et al. 2009 and see Casey et al. 2014 for a more extensive review). These efforts have been paramount for our

[23] Humboldt Research Fellow.

understanding of the IR EBL, but typically suffered from a lack of sensitivity and from source blending due to poor angular resolution.

The advent of the Atacama Large Millimeter/submillimeter Array (ALMA) has opened up a new means to quantify the IR EBL. In particular, the superior sensitivity of ALMA allows for a better quantification of the IR EBL down to fainter limits. This is further aided by a higher angular resolution that can overcome source blending. Indeed, since ALMA started operating, a large number of works in the literature have contributed to better quantifying millimeter and submillimeter number counts (Hatsukade et al. 2013, 2016; Ono et al. 2014; Carniani et al. 2015; Aravena et al. 2016; Fujimoto et al. 2016; Oteo et al. 2016; Dunlop et al. 2017; Umehata et al. 2017; Franco et al. 2018; Muñoz Arancibia et al. 2018; González-López et al. 2020). Aravena et al. (2016), Fujimoto et al. (2016), and Muñoz Arancibia et al. (2018) have pushed the quantification of 1.2 mm number counts down to flux densities of 0.3 and 0.02 mJy, respectively. Fujimoto et al. (2016) reached this conclusion by taking advantage of lensing through a cluster. More recently, Muñoz Arancibia et al. (2018) also measured the number counts of galaxies at 1.1 mm down to 0.01 mJy, taking advantage of lensing. Although focusing on lensed sources has proven to be an efficient way to reach faint flux densities, uncertainties in the lensing model complicate the precise derivation of the faint number counts. Aravena et al. (2016) on the other hand reached flux densities of 0.3 mJy as part of the ASPECS pilot project (Walter et al. 2016), targeting the 1.2 mm emission in a contiguous blank region on the sky corresponding to $\sim$1 arcmin^2.

González-López et al. (2020) present the deepest 1.2 mm continuum images obtained to date in a contiguous area over the sky (4.2 arcmin^2), reaching number count statistics down to an rms flux density of 9.5 μJy per beam. This work was based on the band 6 component of the full ASPECS survey, whose first results were presented in Aravena et al. (2019), Boogaard et al. (2019), Decarli et al. (2019), González-López et al. (2019), and Popping et al. (2019). González-López et al. (2020) found that the 1.2 mm number counts flatten below flux densities of $\sim$0.3 mJy. These results are similar to the earlier findings at less significance by Muñoz Arancibia et al. (2018) based on lensed submillimeter emission in three galaxy clusters. González-López et al. (2020) was furthermore able to decompose the 1.2 mm number counts in bins of different galaxy properties (redshift, stellar mass, star formation rate, and dust mass). Now that the shape and normalization of the 1.2 mm number counts are well characterized by ALMA, as well as how these decompose in bins of different galaxy properties, it is crucial to put these observations in a theoretical framework.

In this paper, we present a new semiempirical approach to model the 1.1 mm and 850 μm number counts of galaxies. This model is designed to explore how the number counts are built up by contributions from galaxy samples at different redshifts and varying galaxy properties (i.e., the star formation rate (SFR), stellar mass, and dust mass). In particular, we aim to address the cause for the flattening in the 1.2 mm number counts of galaxies, and if a similar flattening is to be expected in the 850 μm number counts. To this aim, we explore which galaxies are responsible for different parts of the (sub)millimeter number counts of galaxies. Based on our findings, we furthermore discuss the best strategies to detect large numbers of galaxies through their dust continuum.

The paper is outlined as follows. We present the model in Section 2. We present the predictions by the model and how they compare to and explain the observational data in Section 3. We discuss our findings in Section 4 and summarize them and draw conclusions in Section 5. Throughout this paper, we adopt a flat ΛCDM cosmology, with parameters ($\Omega_M = 0.307$, $\Omega_\Lambda = 0.693$, $h = 0.678$, $\sigma_8 = 0.823$, and $n_s = 0.96$), similar to *Planck* 2018 constraints (Planck Collaboration et al. 2018). We furthermore adopt a Chabrier (2003) stellar initial mass function.

2. Model Description

This section describes our methodology to predict the submillimeter continuum flux density of galaxies. In summary, we start with mock light cones (i.e., a continuous model galaxy distribution from $z = 0$ to $z = 10$ over an area on the sky) created by the `UniverseMachine` (Behroozi et al. 2019), which assigns galaxy properties (stellar mass, SFR) to halos based on observationally constrained relations. We then use a number of empirical relations to assign dust masses to each galaxy. We calculate the 850 μm and 1.1 mm flux density of galaxies following the fits presented in Hayward et al. (2011, 2013a) as a function of galaxy SFR and dust mass.

2.1. Generating Mock Light Cones

The UniverseMachine is an empirical model of galaxy formation that infers how the SFRs of galaxies depend on host halo mass, halo mass accretion rate, and redshift via forward modeling (Behroozi et al. 2019). Given a guess for the SFR–halo relationship, the UniverseMachine applies the relationship to a dark matter halo catalog and generates an entire mock universe. This mock universe is observed in the same way as the real universe, and galaxy statistics (including stellar mass functions, specific SFRs, galaxy clustering, luminosity functions, and quenched fractions, among others) are compared to evaluate the likelihood for the given SFR–halo relationship to be correct. This likelihood is then fed to a Markov Chain Monte Carlo algorithm that explores the posterior distribution of SFR–halo relationships that match observations. The model was compared to galaxy observations from, among others, the SDSS, PRIMUS, CANDELS, zFOURGE, and ULTRAVISTA surveys over the range $z = 0$ to $z = 10$; for full details of the modeling and data, see Behroozi et al. (2019). The underlying dark matter simulation was Bolshoi–Planck, which resolves halos down to $10^{10}\,M_\odot$ (hosting galaxies down to $10^7\,M_\odot$) in a periodic cosmological region that is 250 Mpc h^{-1} on a side (Klypin et al. 2016; Rodríguez-Puebla et al. 2016). Halo finding and merger tree construction were performed by the Rockstar and Consistent-Trees codes, respectively (Behroozi et al. 2013b, 2013c).

The light cones used in this paper are based on the best-fit UniverseMachine DR1 SFR–halo relationship. This relationship was used to generate a mock catalog containing galaxy stellar masses and SFRs for every halo (and subhalo) in Bolshoi–Planck at every redshift output (180, equally spaced in log a from $z \sim 20$ to $z = 0$). Eight light cones were generated for the CANDELS GOODS-S field footprints by choosing random locations within the simulation volume and then selecting halos along a random line of sight, tiling the periodic simulation volume as necessary. When selecting halos, the cosmological distance along the light cone was used to determine the closest simulation redshift output to use. The final light cones include

galaxy stellar masses, SFRs, sky positions, and redshifts (including both cosmological redshift and redshift due to peculiar velocities), as well as full dark matter halo properties.

2.2. Assigning (Sub)millimeter Luminosities to Galaxies

Hayward et al. (2011, 2013b) presented fitting functions for the (submillimeter) flux densities of galaxies based on their SFR and dust mass. These fitting functions were derived by running the SUNRISE (Jonsson 2006) dust radiative transfer code on smoothed particle hydrodynamics simulations of isolated and merging galaxies. The authors found that the 850 μm and 1.1 mm flux density of IR-bright galaxies (down to 0.5 mJy) can be well described by

$$S_{850\,\mu\mathrm{m}} = 0.81\ \mathrm{mJy}\left(\frac{\mathrm{SFR}_{\mathrm{obscured}}}{100\ M_{\odot}\ \mathrm{yr}^{-1}}\right)^{0.43}\left(\frac{M_d}{10^8\ M_{\odot}}\right)^{0.54}, \quad (1)$$

and

$$S_{1.1\ \mathrm{mm}} = 0.35\mathrm{mJy}\left(\frac{\mathrm{SFR}_{\mathrm{obscured}}}{100\ M_{\odot}\ \mathrm{yr}^{-1}}\right)^{0.41}\left(\frac{M_d}{10^8\ M_{\odot}}\right)^{0.56}, \quad (2)$$

where $S_{850\,\mu\mathrm{m}}$ and $S_{1.1\ \mathrm{mm}}$ mark the 850 μm and 1.1 mm flux density, and $\mathrm{SFR}_{\mathrm{obscured}}$ and M_d the dust-obscured SFR of galaxies and dust mass of a galaxy, respectively. Hayward et al. (2011) find that these functions recover the submillimeter flux (brighter than 0.5 mJy) at these wavelengths of simulated galaxies to within a scatter of 0.13 dex in the redshift range $z \sim 1$–6 (we include this scatter when we calculate fluxes). The apparent redshift independence of this relation is a natural result of the negative k-correction in the millimeter range of the galaxy spectral energy distribution. This fit underpredicts the flux of galaxies significantly at $z < 0.5$. Because of the change in normalization of the main sequence of star formation from $z = 0.5$ to $z = 0$ (e.g., Speagle et al. 2014), we do not expect these galaxies to contribute significantly to the total submillimeter flux density (as we will see in Section 3.2). Furthermore, the volume probed by a survey in the redshift range $z = 0$–0.5 is only a small fraction of the total volume from $z = 0$ to $z = 8$.[24] We furthermore do not include a correction for the cosmic microwave background (CMB) as a background radiation field in this work. Our methodology does not provide the actual dust temperature of the simulated galaxies, from which a correction factor can be estimated following da Cunha et al. (2013). If we assume a dust temperature of 20 K, we expect that 90% of the intrinsic flux emitted by galaxies at $z = 3$ is observed against the CMB background. There have been works suggesting that the dust temperature of galaxies evolves to even higher temperatures (40 K and above at $z > 3$) as a function of lookback time (e.g., Bouwens et al. 2016; Narayanan et al. 2018). At these temperatures, more than 95% of the intrinsic flux is observed against the CMB background at $z < 5$. We are therefore confident that (at least for the regime where we can directly compare our model to observations) the CMB will not alter our results significantly.

[24] Our results regarding the flattening of the number counts are not sensitive to the uncertainties in the estimated flux within the $z = 0$–0.5 redshift range. Even in the extreme scenario where the predicted fluxes at $z < 1$ are too low by an order of magnitude, we still recover the flattening in the number counts (see also the redshift distribution of the number counts in Figure 3).

The dust-obscured SFR can be described as

$$\mathrm{SFR}_{\mathrm{obscured}} = f_{\mathrm{obscured}}\,\mathrm{SFR}_{\mathrm{total}}, \quad (3)$$

where f_{obscured} corresponds to the obscured fraction of star formation and $\mathrm{SFR}_{\mathrm{total}}$ corresponds to the total SFR of galaxies (the sum of the obscured and unobscured fraction). To calculate f_{obscured}, we use the empirical relation derived by Whitaker et al. (2017) between the obscured fraction of star formation and the stellar mass for main-sequence galaxies in the redshift range from $z = 0.5$ to $z = 2.5$. We assume that this empirical fit extends toward higher redshift and also applies for galaxies above the main sequence. Hayward et al. (2013b) do not make an explicit distinction between unobscured and obscured star formation in their fitting functions (i.e., they implicitly assume that all star formation is dust obscured). To quantify the effect of introducing the parameterization by Whitaker et al. (2017), we explore the scenario where f_{obscured} is set to 1 in Appendix A. We find that the predicted number counts are almost identical to the predictions by our fiducial.

To calculate the dust mass M_d of galaxies, we use a strategy similar to the one presented in Hayward et al. (2013a). We first calculate the total gas mass of galaxies as described in Popping et al. (2015a). The authors determine gas masses for galaxy catalogs generated using subhalo abundance matching models. In summary, the authors calculate what gas mass a galaxy must have to have an SFR equal to the SFR obtained from the subhalo abundance matching model. This is done by randomly picking a gas mass for a galaxy and assuming that the gas and stellar mass of this galaxy are distributed exponentially, with a scale length given by the stellar mass–size relation of galaxies as found by van der Wel et al. (2014). At every point in the disk, the gas is then divided into a molecular and an atomic component, following the empirical relation determined by Blitz & Rosolowsky (2006), which relates the midplane pressure acting on the gas disk to the molecular hydrogen fraction. The SFR surface density is then calculated as a function of the molecular hydrogen surface density following Bigiel et al. (2008), but allowing for an increased star formation efficiency in high surface density environments. The total SFR of a galaxy is calculated by integrating over the entire disk. The "true" gas mass of a galaxy is determined by iterating over gas masses until the SFR calculated following these empirical relations equals the SFR provided by the subhalo abundance matching model. A more detailed description of this method is given in Popping et al. (2015a, 2015b).

Once the total cold gas mass of a galaxy is known, we estimate the dust mass of this galaxy by multiplying it with a dust-to-gas ratio. We use the fit presented in De Vis et al. (2019) between the dust-to-gas ratio and gas-phase metallicity of galaxies of local galaxies to estimate a dust-to-gas ratio. Theoretical simulations have suggested that the relation between dust-to-gas ratio and gas-phase metallicity hardly evolves between redshifts $z = 0$ and $z = 6$ (e.g., Feldmann 2015; Popping et al. 2017; though see Hou et al. 2019, who suggest that the normalization of the relation between dust-to-gas ratio and gas-phase metallicity decreases at $z > 3$). The gas-phase metallicity of galaxies is estimated as a function of the stellar mass and redshift by fitting the results presented in Zahid et al. (2013; see also Zahid et al. 2014). The metallicities are converted to the same metallicity calibration used in De Vis et al. (2019) following the approach presented in Kewley & Ellison (2008). Zahid et al. (2013) present metallicities

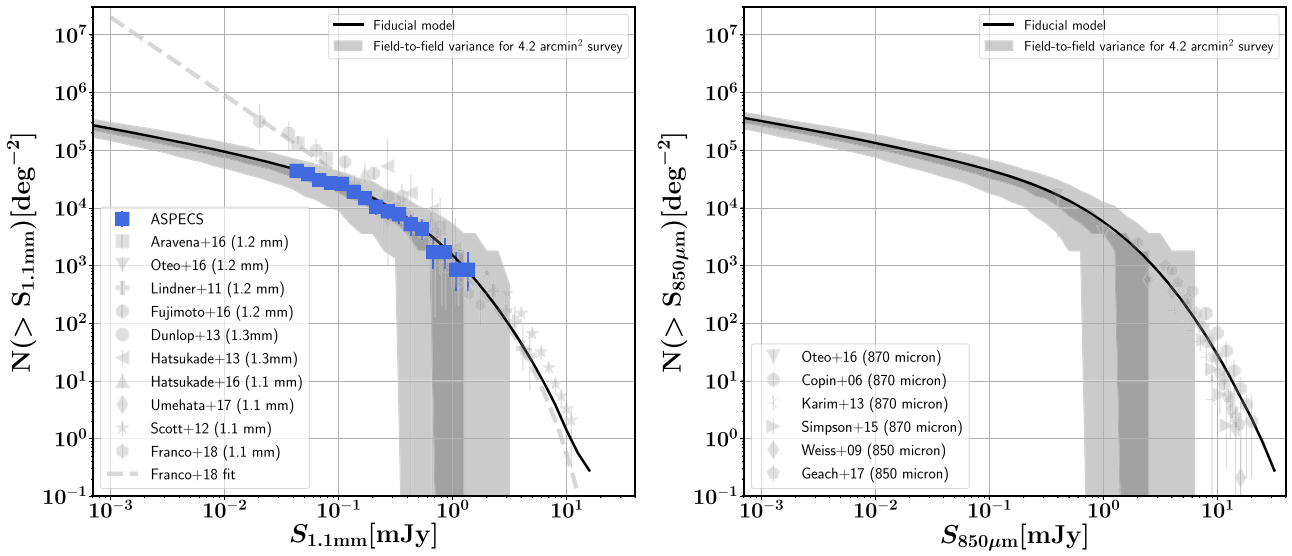

Figure 1. The 1.1 mm (left) and 850 μm (right) galaxy number counts. The black solid lines mark our predictions for the number counts when accounting for all the galaxies in the entire simulated light cone. The dark- and light-gray shaded areas mark the 1σ and 2σ scatter due to field-to-field variance, assuming a survey with the size of ASPECS (i.e., 4.2 arcmin^2). The model predictions are compared to a literature compilation of number counts, where the dashed line corresponds to the Schechter fit presented by Franco et al. to their literature compilation. The blue points show the number counts derived from ASPECS (González-López et al. 2020).

for a sample of galaxies out to $z \sim 2.26$, and we assume that the redshift-dependent fit to the mass–metallicity relation extends toward higher redshifts. A similar approach was also adopted by Imara et al. (2018) to assign dust masses to galaxies based on empirical scaling relations.

Throughout this process, we use the stellar mass and SFR predicted by the UniverseMachine as input for the empirical relations. To account for the fact that empirical relations are based on observationally derived stellar masses and SFRs and not on the intrinsic stellar mass and SFR of a galaxy, we make use of the predictions for galaxy properties from the UniverseMachine that account for observational effects and errors. Each of the adopted empirical relations has an intrinsic error associated with it. To account for this, we run 100 realizations of the model, sampling over errors in the empirical relations. In Appendix A, we explore alternative empirical relations with the aim of developing a sense of how robust our results are against our assumptions. We do not account for blending effects and gravitational lensing when modeling number counts as our analysis focuses on flux densities for which blending is not thought to significantly contribute to the number counts (e.g., Hayward et al. 2013a).

To test the validity of our model, we compare the 1.1 mm flux predicted for the galaxies observed in González-López et al. (2020) based on their observed stellar mass, SFR, and redshift to the observed fluxes. We find that the mean ratio between the predicted and observed 1.1 mm flux densities for these objects is 1.05, with a standard deviation of 0.81.

3. Results

In this section, we present our predictions for the 1.1 mm and 850 μm number counts of galaxies, specifically focusing on how they compare to current observations and which galaxies are responsible for the number counts at different flux densities. Throughout this paper, we compare our model predictions to a set of observations taken from Coppin et al. (2006), Weiß et al. (2009), Lindner et al. (2011), Scott et al. (2012), Hatsukade et al. (2013, 2016), Karim et al. (2013), Simpson et al. (2015), Aravena et al. (2016), Dunlop et al. (2017), Fujimoto et al. (2016), Oteo et al. (2016), Umehata et al. (2017), Geach et al. (2017), Franco et al. (2018), and González-Løpez et al. (2020, the deepest survey at 1.2 mm over a contiguous area on the sky to date). This compilation includes observations based on single-dish instruments as well as with ALMA. These observations were carried out over a range of wavelengths and scaled to 1.1 mm and 850 μm fluxes such that $S_{1.1\,\mathrm{mm}}/S_{1.2\,\mathrm{mm}} = 1.36$, $S_{1.1\,\mathrm{mm}}/S_{1.3\,\mathrm{mm}} = 1.79$, and $S_{870\,\mu\mathrm{m}}/S_{850\,\mu\mathrm{m}} = 0.92$, assuming a dust emissivity index $\beta = 1.5$–2.0 (e.g., Draine 2011) and a temperature of 25–40 K (e.g., Magdis et al. 2012; Schreiber et al. 2018). We first present the model number counts and how field-to-field variance affects the derived number counts. We then break up the number counts in bins of redshift, dust mass, stellar mass, and SFR. We finish by showing the redshift distribution of galaxies compared to observations.

3.1. The (Sub)millimeter Number Counts of Galaxies and Field-to-field Variance

We present the 1.1 mm and 850 μm flux density number counts of galaxies in Figure 1 (black solid lines). The number counts predicted by the model are in good agreement with the ASPECS data, both at 1.1 mm and at 850 μm over the full flux density range where observations are available. We predict a flattening in the number counts of galaxies for flux densities below $\sim$0.3 mJy at 1.1 mm, similar to the flattening found by González-López et al. (2020). We also find a flattening in the 850 μm number counts around a flux density of $\sim$1 mJy. The predicted number counts lie below the observations by Fujimoto et al. (2016), who derived their number counts based on uncertain lensing models. Aravena et al. (2016) calculated their number counts based on a significantly smaller area and simpler analysis techniques. A more detailed description of the source of the discrepancy is given in González-López et al. (2020).

As one of the specific aims of this paper is to assess the origin of the flattening in the 1.1 mm number counts detected by González-López et al. (2020), we show the number counts

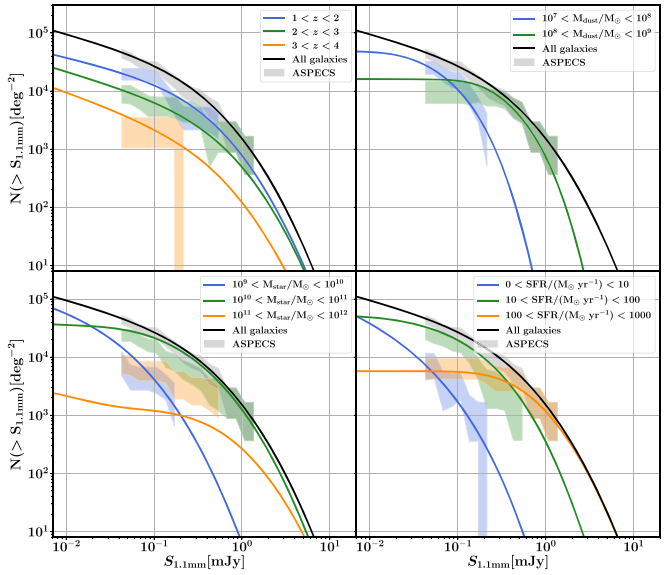

Figure 2. The predicted and observed 1.1 mm galaxy number counts in bins of redshift (top left), dust mass (top right), stellar mass (bottom left), and SFR (bottom right). The solid lines correspond to the model predictions, whereas the shaded areas show the ASPECS observations.

derived for the entire simulated area, as well as the number counts derived for a simulated area corresponding to the ASPECS survey. To this aim, we calculate the number counts in 100 randomly drawn sub-areas covering 4.2 arcmin^2 (the area covered by ASPECS) on the sky. The number counts of the full simulated volume are depicted as a black solid line, whereas the 1σ and 2σ scatter when calculating the number counts in the areas corresponding to ASPECS are depicted as gray shaded regions. There are two noteworthy results with regard to cosmic variance. First of all, at flux densities fainter than 1 (3) mJy when focusing on 1.1 mm (850 μm) emission, the typical 2σ scatter due to field-to-field variance is only a factor of 1.5 and the flattening in the number counts is always recovered. Second, due to the small area covered, sources brighter than 1 mJy (at 1.1 mm, 3 mJy at 850 μm) are typically missed by surveys targeting only 4.2 arcmin^2 on the sky (see also Figure 9).

3.2. Which Galaxies are the Main Contributors to the Number Counts?

The depth of the ASPECS survey combined with the rich ancillary data available in the HUDF allowed González-López et al. (2020) to decompose the observed 1.2 mm number counts in bins of stellar mass, dust mass, SFR, and redshift. We compare our model predictions to these observations in Figure 2. We find a decent agreement between the observations and model predictions when breaking up the number counts in bins of redshift, dust mass, and SFR. When breaking up the number counts in bins of stellar mass, we find that the contribution of galaxies with stellar masses between 10^9 and $10^{10}\,M_\odot$ is well reproduced. Our model predicts a contribution to the number counts below 0.5 mJy by galaxies with a stellar mass between 10^{10} and 10^{11} solar masses that is too large (up to a factor of 2). The predicted contribution by galaxies with larger stellar masses in this flux density range is too small (up to a factor of 3) compared to the observations. Tests have shown that when we change the stellar mass bins (e.g., from $10^{10.5}$ to $10^{11.5}\,M_\odot$), the agreement between models and observations is much better. This suggests that the discrepancy is (at least partially) driven by uncertainties in the observed stellar masses that can easily be of the order 0.3 dex (Leja et al. 2019). We have furthermore not taken the effects of cosmic variance into account in this comparison, which can be nonnegligible for the bins with the highest stellar masses (Moster et al. 2011; because the ASPECS survey only covers an area of 4.2 arcsec^2 in ALMA band 6). The good agreement between the model predictions is encouraging and opens up the opportunity to explore the model further to better understand which galaxies contribute to the number counts at different flux densities.

We show the number counts of galaxies in different redshift bins in Figure 3. Galaxies at $z > 3$ make up for a small fraction of the total number counts at 1.1 mm and 850 μm. The number counts are made up by an equal contribution of galaxies in the redshift range $z = 2$–3 and $z = 1$–2 for flux densities brighter than $\sim$3 ($\sim$6) mJy at 1.1 mm (850 μm). At lower flux densities, the largest contribution to the number counts comes from galaxies in the redshift bin $z = 1$–2. Galaxies at $z < 1$ hardly contribute to the number counts at flux densities larger than $\sim$0.1 mJy at both wavelengths, whereas they contribute more importantly to the number counts at fainter fluxes (although still a factor of 2 less than galaxies at $z = 1$–2). There is a clear flattening visible in the number counts of galaxies at all redshifts. The galaxy population that contributes most to the total (all redshifts) number counts at flux densities of 0.3 mJy at 1.1 mm (1 mJy at 850 μm; this corresponds to the flux density below which the total number counts rapidly flatten) consists of galaxies with redshifts in the range $z = 1$–2.

In Figure 4, we show the number counts of galaxies in bins of stellar mass. As the flux density increases, the number counts are dominated by more massive galaxies. This is a natural consequence of an increase in the dust mass and SFR of galaxies as a function of stellar mass. Galaxies with stellar masses around $5 \times 10^{10}\,M_\odot$ contribute most dominantly to the number counts at the flux density below which the number counts flatten (0.3 and 1 mJy at 1.1 mm and 850 μm, respectively).

We show the number counts of galaxies in bins of SFR in the middle row of Figure 4. Not surprisingly, we find that the number counts at the brightest flux densities probed by observations are dominated by the most actively star-forming galaxies (i.e., SFR $> 100\,M_\odot$ yr^{-1}). Interestingly, at $\sim$0.25 (0.6) mJy, the 1.1 mm (850 μm) number counts are driven by an equal contribution from galaxies with an SFR in the bin between 10–50, 50–100, and 100–500 $M_\odot$ yr^{-1}. This pivoting point also roughly marks the location of the flattening in the number counts. At lower flux densities (but brighter than 0.05 and 0.1 mJy for the 1.1 mm and 850 μm number counts, respectively) the number densities are dominated by galaxies with an SFR = 10–50 $M_\odot$ yr^{-1}. At even lower flux densities, galaxies with SFRs between 1 and 5 $M_\odot$ yr^{-1} are predominantly responsible for the number counts. In the previous figures, we noticed that as the flux density increases, the number counts are dominated by more massive galaxies. Such a behavior is not seen for the SFR of galaxies. Some bins in SFR (e.g., 5–10 and 50–100 $M_\odot$ yr^{-1}) are never the dominant population of galaxies responsible for the observed total number counts. This is because the 1.1 mm and 850 μm fluxes of galaxies depend more strongly on dust mass than on SFR (see Equations (2) and (1)).

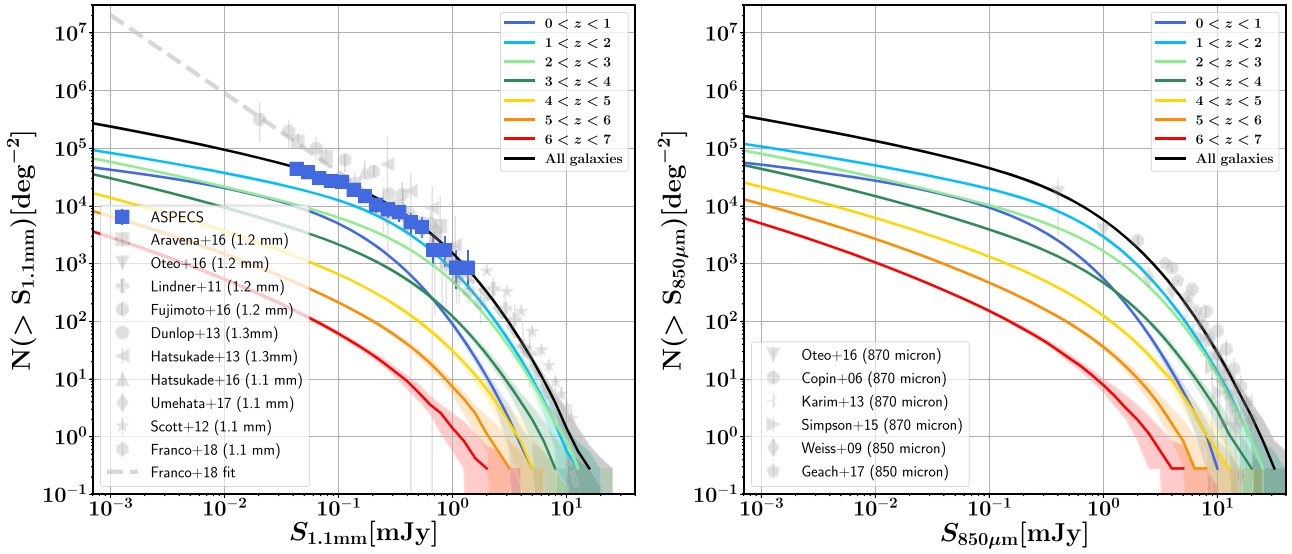

Figure 3. The 1.1 mm (left) and 850 μm (right) galaxy number counts. The black solid lines mark our predictions for the number counts when accounting for all the galaxies in the light cone (as shown in Figure 1). The colored lines mark the number counts when selecting galaxies based on their redshift. The color shading corresponds to the 2σ scatter when sampling over the intrinsic scatter of the empirical scaling relations. The model predictions are compared to a literature compilation of number counts as in Figure 1. The 1.1 mm number counts are dominated by galaxies at $z = 1$–2, with additional contributions from galaxies up to $z = 3$ at the brightest fluxes and galaxies in the range $z = 0$–1 at the faintest fluxes.

The contribution by galaxies with different dust masses to the 1.1 mm and 850 μm number counts is also presented in Figure 4 (bottom row). Similar to the stellar mass, we find that as the flux density increases, the number counts are dominated by galaxies with increasing dust masses. We find that galaxies with dust masses in the range between 10^8 and $10^9\,M_\odot$ contribute most strongly to the number counts at 0.3 (1.0) mJy at 1.1 mm (850 μm), the flux density below which the number counts flatten.

3.3. The Flattening in Number Counts Corresponds to the Knee and Shallow Faint-end Slope of the Dust Continuum Luminosity Functions

In the previous subsection, we have seen that our model and the observations suggest that galaxies at $z = 1$–2 contribute most to the flux densities at which the 1.1 mm and 850 μm number counts flatten (Figure 3). We have furthermore seen that the galaxies responsible for the flattening have stellar masses around $5 \times 10^{10}\,M_\odot$, dust masses between 10^8 and $10^9\,M_\odot$, and SFRs in the range between 10 and $500\,M_\odot\,\mathrm{yr}^{-1}$. At $z = 1$–2, a stellar mass of $5 \times 10^{10}\,M_\odot$ roughly corresponds to the stellar mass at the knee of the stellar mass function at these redshifts (e.g., Tomczak et al. 2014). This suggests that the flattening in the number counts is driven by the shape of the 1.1 mm and 850 μm luminosity function at $z = 1$–2 and that the flattening may actually simply reflect observations probing galaxies below the knee of this function.

To test our hypothesis, we switch from number counts (projected densities on the sky) to volume densities. In Figure 5, we show the luminosity function (number of sources per volume element) predicted from our model as a function of redshift (cosmic time).[25] We also show the stellar mass function and dust mass functions. We highlight the flux density and stellar (dust) mass regime at which the flattening occurs with a vertical gray band. Indeed, the knee of the luminosity function at $z = 1.5$ (in the middle of the redshift range $z = 1$–2) corresponds to the flux densities at which the flattening in the number counts occurs. Similarly, the stellar and dust mass at which the flattening occurs in the number counts corresponds to the knee of the respective mass functions at $z = 1.5$. We furthermore find that the faint-end slope of the dust continuum luminosity functions (and dust mass function) is significantly shallower than the low-mass slope of the stellar mass function (almost flat at $z < 2$; compare the top two panels to the bottom-left panel). This is driven by the strong dependence of the gas-phase metallicity on stellar mass and the strong dependence of the dust-to-gas ratio on the gas-phase metallicity. Because of this shallow slope in the dust continuum luminosity function, integrating to fainter flux densities results in only a modest increase in detected sources, as will be discussed in Section 4. The flattening in the number counts thus corresponds to probing galaxies below the knee of the luminosity function.

Our model assumes that a set of empirical relations can be used to describe the entire population of galaxies from low to high redshifts. It is therefore worthwhile to explore if our finding that the flattening in the number counts is caused by the shape of the dust continuum luminosity function being robust against changes in the assumed empirical relations. In Appendix A of this work, we adopt a variety of different assumptions, including different recipes to assign gas masses to galaxies, different mass–metallicity relations, a different assumption for the amount of star formation that is dust obscured, and different assumptions for the dust-to-gas ratio of galaxies. Every empirical relation used in the model has an error associated with it. To better understand how the error in these components affects the number counts, we run the model 100 times, sampling over the intrinsic error for each empirical relation. The different assumptions change the normalization of the number counts by up to a factor of 2. It furthermore slightly changes the shape of the cumulative number counts. Nevertheless, for none of the explored scenarios does the flattening in the number counts disappear. In other words, this flattening is not driven by changes in the assumptions on how we derive the dust-to-gas ratio of galaxies, their gas mass, the fraction of obscured

[25] These are actually 1.1 mm and 850 μm flux density distribution functions, but for simplicity we call them luminosity functions.

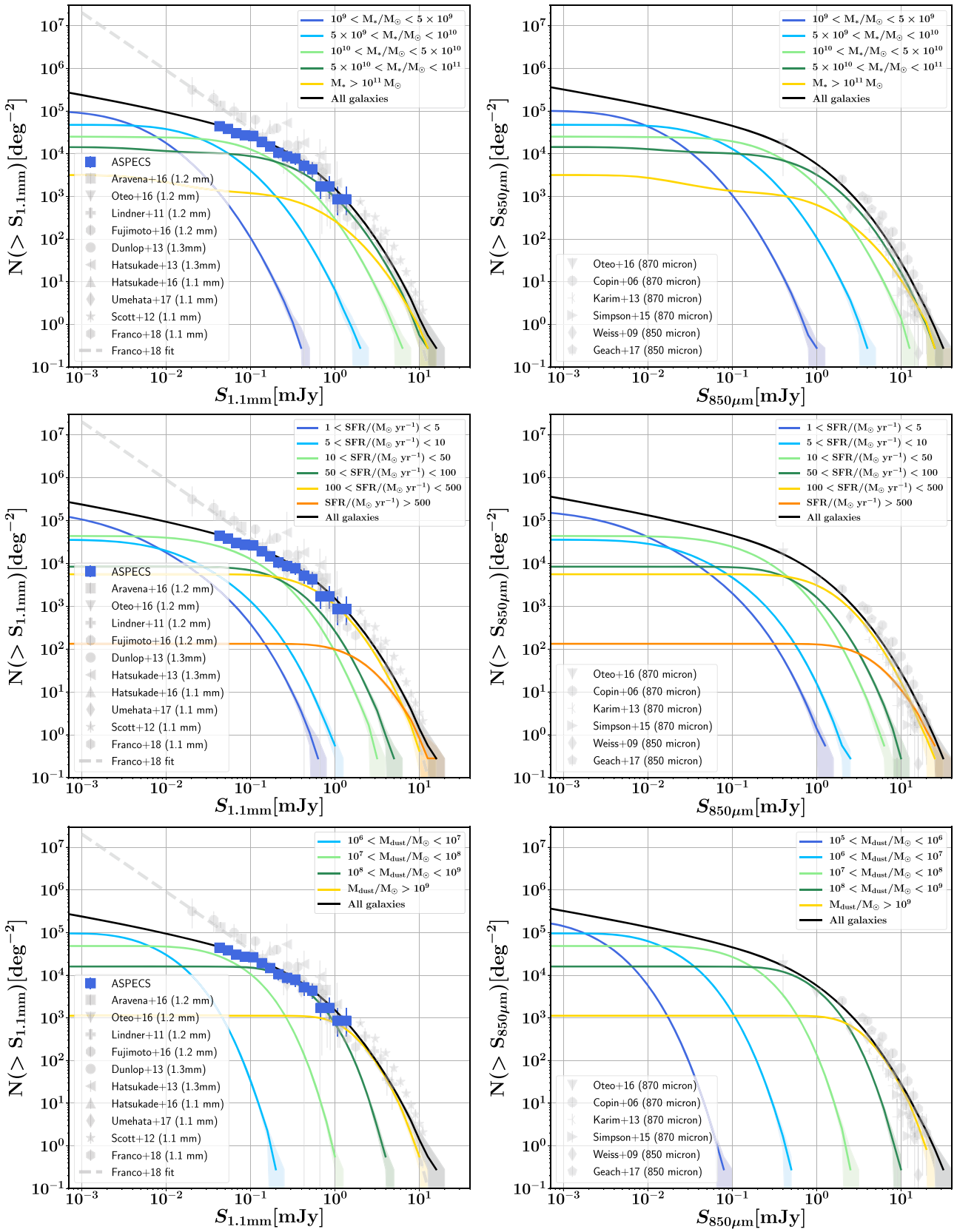

Figure 4. The 1.1 mm (left) and 850 μm (right) galaxy number counts of galaxies, broken up by different galaxy properties (integrated over all redshifts). The black solid lines mark our predictions for the number counts when accounting for all the galaxies in the light cone (as shown in Figure 1). The colored lines mark the number counts when selecting galaxies based on their stellar mass (top row), SFR (middle row), and dust mass (bottom row). The color shading corresponds to the 2σ scatter when sampling over the intrinsic scatter of the empirical scaling relations. The model predictions are compared to a literature compilation of number counts as in Figure 1.

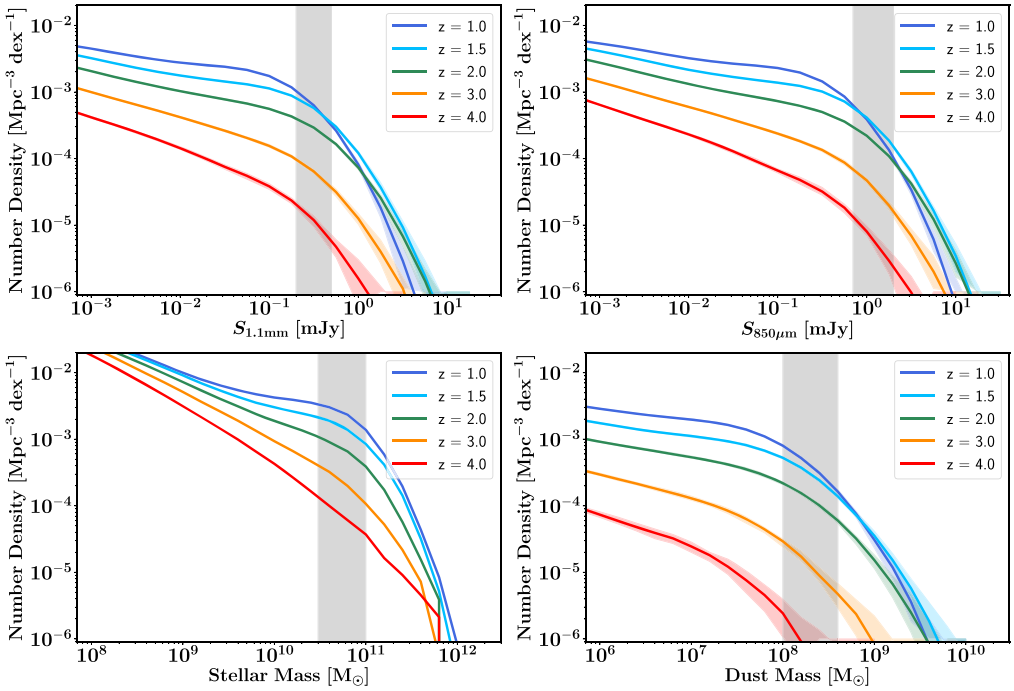

Figure 5. The 1.1 mm luminosity function (top left), the 850 μm luminosity function (top right), the stellar mass function (bottom left), and the dust mass function (bottom right) of galaxies at different redshifts. The color shading corresponds to the 2σ scatter when sampling over the intrinsic scatter of the empirical scaling relations. The gray shaded band in each panel corresponds to the galaxies that contribute most dominantly to flux density at which the predicted flattening starts in the 1.1 mm and 850 μm number counts. The gray bands overlap with the knee of the respective mass/luminosity functions, suggesting that the flattening in number counts is a reflection of the 1.1 mm and 850 μm luminosity functions. We do not show the luminosity and mass functions at $z < 1$ as the predicted flux densities at these redshifts are not reliable.

star formation, their metallicity, or the uncertainties in the individual model components. This strengthens our conclusion that the flattening in the number counts is simply caused by the distribution of the underlying galaxy population, i.e., probing galaxies below the knee of the dust continuum luminosity functions/mass functions.

3.4. Redshift Distribution

Current (sub)millimeter surveys with ALMA have predominantly detected galaxies at redshifts $z < 3.5$ (see, for example, Figure 18 in Franco et al. 2018 and other figures in Aravena et al. 2016, Bouwens et al. 2016, and González-López et al. 2020). Even though ALMA has pushed the detection limit of galaxies to flux densities below 0.1 mJy, the fraction of galaxies at redshifts larger than 3.5 still remains very low. This is driven by the dominant contribution of galaxies at $z = 1$–3 to the number counts (Figure 3).

To quantify the agreement between the redshift distribution of (sub)millimeter detections predicted by our model and the current observations, we present a comparison between the two in Figure 6. For this comparison, we adopt the same field of view and sensitivity cutoff as the observations. We compare our predictions to observational results by Franco et al. (2018) and González-López et al. (2020). These works probe the 1.1 mm number counts over an area of 69 arcmin^2 (Franco et al. 2018) down to 0.874 mJy and an area of 4.2 arcmin^2 down to 0.034 mJy (González-López et al. 2020). To account for field-to-field variance, we calculate the number counts 1000 times over a random portion of the entire modeled light cone covering the same area as the observations (similar to Figure 1). We show the mean and 1σ distribution of the predicted number counts. The predicted redshift distribution at $z < 1$ cannot be fully trusted, as the negative k-correction implied by our model does not apply at these redshifts.

Overall, we find that the observed redshift distributions from González-López et al. (2020) typically all fall within the 1σ scatter of the model predictions. This suggests that, at least at $z < 3$, the model not only successfully reproduces the cumulative number counts of galaxies, but also the redshifts of the sources that are responsible for these number counts. The low number statistics of detections at $z > 4$ makes it hard to further quantify the success of the presented model. Possibly most surprising is the lack of sources detected by Franco et al. (2018) at $z < 2$ compared to our model predictions. We additionally find that at $\sim$1 mJy, our model predicts number counts higher than those derived by Franco et al. (2018). Given the success of our model in reproducing the number counts by González-López et al. (2020), the apparent mismatch with Franco et al. may suggest a tension between the model predictions and observations for the brightest millimeter sources, but we note that not all sources in the Franco et al. (2018) sample have a spectroscopic redshift. Furthermore, a prior-based selection of the data presented in Franco et al. suggested that additional sources may have been missed in the blind selection, which may change the redshift distribution (M. Franco et al. 2020, in preparation). Lastly, it has to be noted that the observations still fall within the 2σ range of the model predictions. Our model predicts a higher median redshift for a survey more similar to Franco et al. (2018) than to González-López et al. (2020; although the median redshift predicted for a survey with the Franco et al. specifics is different from what was observed). This is in agreement with previous findings that the survey depth can significantly alter the redshift distribution, with

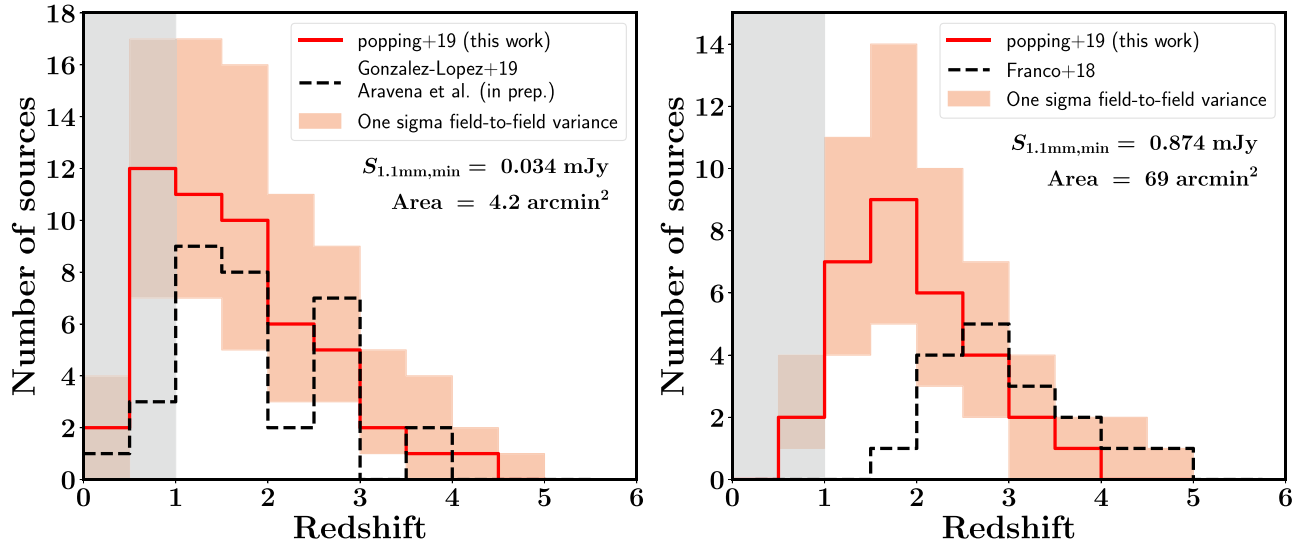

Figure 6. A comparison between the predicted and observed redshift distribution of galaxies observed at 1.1 mm. To account for field-to-field variance, we calculate the number counts 1000 times over a random portion of the entire modeled light cone covering the same area as the observations, imposing the same survey depth (as outlined in the individual panels). The solid line corresponds to the median redshift distribution, whereas the shaded region corresponds to the 1σ scatter. Model predictions are compared to the observations by González-López et al. (2020, left; and M. Aravena et al. 2020, in preparation) and Franco et al. (2018, right). The gray shaded area (at $z < 1$) marks the regime where the model predictions cannot be fully trusted because the negative k-correction does not apply anymore at those redshifts.

shallower surveys yielding higher mean redshifts (Béthermin et al. 2015).

4. Discussion

4.1. Observational Consequences

We have presented a new data-driven model for the cumulative number counts and redshift distribution of (sub) millimeter detections of galaxies. This model successfully reproduces current observations (the cumulative number counts, number counts in bins of different galaxy properties, and redshift distribution functions), including the flattening in the 1.1 mm number counts observed by González-López et al. (2020). There is a simple origin for this flattening, namely the shape of the underlying luminosity function of galaxies at 1.1 mm in the redshift range between $z = 1$ and $z = 2$ (probing the knee and shallow faint-end slope). We have furthermore demonstrated that this conclusion is robust against field-to-field variance and the assumptions made in the presented model. The predicted (and observed) flattening in the number counts has clear consequences for future continuum surveys with ALMA. A survey at 1.1 mm deeper than 0.1 mJy will not significantly increase the number of detected sources per square degree. A similar flattening is to be expected for the 850 μm number counts below 1 mJy, a flux density regime only probed by Oteo et al. (2016) so far. Given our predictions, a future deep survey at 850 μm will detect fewer sources than have naively been expected when extending a simple fit to the current 850 μm number count observations.

We can further quantify this by looking into the expected results of hypothetical surveys. In Figure 8, we show the expected number of sources for a survey covering a given area to a given depth. We furthermore show how many hours per pointing it takes to reach that depth (adopting a signal-to-noise ratio of 3 and assuming standard ALMA assumptions in the respective bands with 50 antennas), and how many pointings are needed to cover the targeted area adopting Nyquist sampling. On the top two panels, we also plot contours that mark a fixed number of expected detections. As expected, an increase in area and an increase in depth both result in a larger number of detected galaxies. Below 0.1 mJy (for 1.1 mm, 0.3 mJy for 850 μm), the contours for a constant number of sources are almost horizontal (i.e., they scale less strongly with sensitivity than with area). An increase in depth from 0.1 to 0.01 mJy only results in an increase of a factor of $\sim$3 in the detected number of sources. An increase of the area with an order of magnitude naturally results in an increase of a factor of 10 in the detected number of sources. This suggests that if the goal of the survey is to detect a large number of sources for better statistics, an increase in area is more effective than an increase in survey depth once one has reached a depth of $\sim$0.1 mJy at 1.1 mm ($\sim$0.3 mJy at 850 μm).

In the bottom two panels of Figure 8, we show contours of fixed total on-source time necessary to perform such a survey. This clearly shows that to detect a large number of sources for proper statistics, a wide survey is more time efficient than a deep survey. Figure 8 also shows that although galaxies are intrinsically brighter at 850 μm, a survey at 1.1 mm is actually more time efficient. Because the primary beam of ALMA at 1.1 mm is larger than at 850 μm, within a fixed time, a survey at 1.1 mm can detect fainter sources over a given area than a survey at 850 μm (as the time is distributed over fewer pointings and thus a fainter sensitivity limit can be reached). The number of expected detected sources per arcmin^2 is roughly the same between a survey at 850 μm and 1.1 mm for a fixed on-source observing time.

In Figure 9, we plot the redshift distribution of galaxies per arcmin^2 for surveys reaching different depths. We explore the redshift distribution when accounting for galaxies with flux densities brighter than 0.01, 0.1, and 1 mJy. We mark the redshift range $z < 1$ with a gray vertical band, as the negative k-correction assumed in our model does not apply for this redshift range.

As the depth of the survey increases, the number of galaxies per arcmin^2 increases at every redshift. The number of galaxies detected per arcmin^2 is systematically higher at 850 μm than at 1.1 mm by a factor of 3 for a survey down to 1 mJy and a factor of 1.5 for a survey down to 0.1 mJy and 0.01 mJy. This is the natural consequence of the shape of the (sub)millimeter SED of galaxies, i.e., lower flux densities at longer wavelengths. Interestingly enough, the median redshift of the redshift distributions is very similar for all three survey depths (around $z = 1.5$; although note that the uncertain $z < 1$ redshift range at which our model may overpredict the brightness of sources is included). This seems in tension with observational results (e.g., the higher median redshift of Franco et al. 2018 over that of González-López et al. 2020), similar to what we saw in Figure 6.

At 1.1 mm, a survey reaching a depth of 0.1 mJy will detect approximately an order of magnitude more sources at $1 < z < 4$ (up to a factor of 30 at $z \sim 5$) than a survey reaching a depth of 1 mJy. An increase in sensitivity down to 0.01 mJy yields another factor of $\sim$3 increase in the number of galaxies per arcmin^2 at $z > 1$. At 850 μm a survey with a depth of 0.1 mJy will detect a factor of 8–10 more galaxies than a survey with a depth of 1 mJy at $z > 1$. An additional factor of 2 can be gained by integrating down to a sensitivity of 0.01 mJy. This again emphasizes that below flux densities of 0.1 (0.3) mJy at 1.1 mm (850 μm), the number of expected sources only moderately increases with increasing survey depth. At those densities, a survey is probing the faint-end slope of the dust continuum luminosity function (top two panels of Figure 5).

Summarizing, to significantly increase the number of sources with dust continuum counterparts, a wide survey at 1.1 mm at a flux density of $\sim$0.1 mJy is most cost efficient. A gain of only a factor of 10 in the number of detected sources compared to the results of González-López et al. (2020) could already heavily increase the constraining power for models. Not only will it improve the high-redshift statistics (currently poorly understood), it is also a better approach to obtain dust continuum counterparts of as many objects as possible that are already detected through optical and near-IR surveys in common legacy fields. This will allow a more detailed breakdown of number counts over different galaxy properties as suggested in this work (e.g., as a function of stellar mass and SFR) and a dust-continuum-based gas and dust mass estimate for an increasingly large number of galaxies (e.g., Aravena et al. 2016; Scoville et al. 2016; B. Magnelli et al. 2019, in preparation). The exact survey strategy will ultimately depend on the scientific requirements.

4.2. What a Successful Empirical Model Says about Galaxy Scaling Relations

Our semiempirical model combines a data-driven model for the stellar mass and SFR population of galaxies over cosmic time (Behroozi et al. 2019) with a number of empirical relations to connect the SFR and stellar mass of galaxies to their dust continuum emission. It is comforting to realize that this combination correctly reproduces the observed 1.1 mm and 850 μm number counts. What this teaches us is that the adopted scaling relations all seem to hold at least over the redshift regime $z = 0$–2 (i.e., the redshift range that most dominantly contributes to the number counts). This is especially relevant for the adopted relation between dust-to-gas ratio and gas-phase metallicity and the scaling between dust mass, SFR, and 1.1 mm and the 850 μm dust continuum flux density, as these relations have only been observationally probed in this redshift range for a limited number of massive galaxies (e.g., Aravena et al. 2016, 2019; Dunlop et al. 2017; Miettinen et al. 2017; B. Magnelli et al. 2019, in preparation). We have indeed seen (see Appendix A) that a different choice for the dust-to-gas ratio and mass–metallicity relation results in poorer agreement between the model predictions and observations. It is furthermore encouraging to see that that the Hayward et al. fitting relations for the dust continuum emission of galaxies result in good agreement with observed number counts, even though these fitting relations were derived for galaxies with flux densities brighter than 0.5 mJy.

Except for the redshift range between $z = 1$–2, the constraining power of number counts for our understanding of galaxy physics over cosmic time is rather limited. The fact that our model successfully reproduces the redshift distribution of 1.1 mm detections up to $z = 4$ (within 1σ) is encouraging, but the low number statistics in the $z = 2$–4 redshift range does not allow us to make further claims on the validity of the adopted scaling relations in that redshift regime. It is even harder to make any claims about the physics at higher redshifts. For example, the contribution of galaxies at $z > 4$ to the number counts is very limited, and an order of magnitude increase or decrease in the number of dusty galaxies at $z > 4$ would not change the cumulative number counts significantly. This suggests that we have almost exhausted what can be learned about galaxy physics from cumulative number counts. It is therefore important that future observations start to probe the luminosity function of galaxies at discrete redshifts (and possibly the dust mass function), start connecting the dust continuum measurement to other galaxy properties, and furthermore aim at resolving the interiors of galaxies at submillimeter wavelengths. This requires, among other things, complete spectroscopic redshift samples for sizable numbers of (submillimeter) galaxies. Besides confirming our theoretical hypothesis about the flattening caused by the knee of the mass/luminosity functions at $z = 1$–2 and the shallow faint-end slope, such an effort will provide stringent constraints currently missing for theoretical models that started to include the detailed tracking of dust formation and destruction over cosmic time (McKinnon et al. 2017; Popping et al. 2017; Davé et al. 2019; Hou et al. 2019). These include not only constraints on the dust mass function and cosmic density of dust (e.g., Pozzi et al. 2020; Magnelli et al. 2020), but also the connection between stellar mass and SFR and dust properties. An approach to observationally probe the luminosity function would be to cross-correlate the securely detected dust continuum sources with information from spectroscopic surveys of the UDF, for example, with MUSE (Inami et al. 2017; Boogaard et al. 2019) or based on ALMA spectral information (González-López et al. 2019).

4.3. A Top-heavy Initial Mass Function?

Previous theoretical works have suggested that a top-heavy IMF in starburst environments is necessary to reproduce the number count of bright galaxies while simultaneously reproducing the optical and near-IR properties of galaxies (e.g., Baugh et al. 2005; Lacey et al. 2016). Recent observations of active star-forming regions (analogs of high-redshift starbursts) in our Galaxy and the Large Magellanic Cloud (Motte et al. 2018; Schneider et al. 2018) have suggested that the newly formed stars in these regions indeed have a top-heavy IMF compared to a Chabrier IMF. Zhang et al. (2018) looked at the abundance

ratio of isotopologues (an index of the IMF; Romano et al. 2017) in $z = 2$–3 dust-enshrouded starbursts and concluded that these galaxies have an IMF more top-heavy than a Chabrier IMF.

We find that we can reproduce the number counts of galaxies at 1.1 mm and 850 μm (up to a few tens of mJy at 850 μm) under the assumption of a uniform Chabrier (2003) IMF. This is in line with other recent theoretical efforts that suggest that the number counts of submillimeter-bright galaxies can be reproduced without invoking a top-heavy IMF (e.g., Safarzadeh et al. 2017; Lagos et al. 2019). This does not necessarily mean that starburst environments cannot form stars following a different IMF than Chabrier. It suggests that changes in the IMF in order to match submillimeter number counts are degenerate with other ingredients and predictions of galaxy formation models such as the treatment of dust and dust emission and/or the SF properties of galaxies. These degeneracies should be explored with care.

4.4. Comparison to Earlier Work

There have been multiple theoretical efforts in the literature (some of them from first principles, others adopting a semiempirical approach similar to our model) that model the (sub)millimeter number counts of galaxies. Pre-ALMA, the focus of these comparisons was on the submillimeter galaxies that are orders of magnitude brighter than the sources discussed in this work. Only after ALMA started operations did these comparisons start to include sources with flux densities below 1 mJy.

Somerville et al. (2012) presented predictions for the 850 μm number counts down to 0.01 mJy, based on a semianalytic model of galaxy formation (Somerville et al. 2008). This model predicts a sharp drop in the differential number counts of galaxies for flux densities below 0.1 mJy. The model does not succeed in reproducing the observational constraints that were available at that time.

Cowley et al. (2017) use a different semianalytic model to study 850 μm number counts of galaxies. The authors reproduce the observations and predict a flattening in the number counts, but do not explore what causes this flattening. The authors specifically focus on the effect of field-to-field variance on observed number counts and, similar to us, find that survey design influences how well the underlying "real" number count distribution of galaxies is recovered.

Lacey et al. (2016) provide predictions for the 850 μm number counts using the same semianalytic model as Cowley et al. (2017). The authors specifically explore how different prescriptions for the baryonic physics in galaxies affect the number counts, but found all explored prescriptions predict a flattening in the number counts. This strengthens our conclusion that the flattening is caused by the underlying galaxy population. The authors furthermore explore the redshift distribution of submillimeter-detected galaxies, but focus on surveys with a depth of 5 mJy. In order to reproduce the observed number counts (especially for the brightest flux densities), Lacey et al. (2016) adopt a top-heavy IMF during starburst events (see also Baugh et al. 2005). Our work on the other hand suggests that the number counts can be reproduced by a simple semiempirical model that does not need to make any changes to the initial mass function of the stars.

Safarzadeh et al. (2017) present predictions for the 850 μm number counts of galaxies based on a semianalytic model (Lu et al. 2011, 2014). In this work, the authors calculate the 850 μm flux of galaxies by coupling the SAM output to the fitting functions presented in Hayward et al. (2013b). The presented predictions agree fairly well with the observations that were available at that time (although they seem to predict higher number densities than found by Aravena et al. 2016 after rescaling to 850 μm). The model predictions include a flattening of the cumulative number counts below 850 μm flux densities $\sim$1 mJy, in rough agreement with our predictions. The main result of Safarzadeh et al. (2017) is that the observed 850 μm number counts can be reproduced by the models without invoking the need for a top-heavy IMF, in line with our findings. This also agrees with the findings, using a different semianalytic model, by Lagos et al. (2019), who reach a similar conclusion by predicting the 850 μm flux density directly from the star formation history of the galaxies with a physical model for attenuation.

Hayward et al. (2013b) couple a semiempirical model with the fitting functions from Hayward et al. (2011) to model the number counts at 1.1 mm at flux densities brighter than 0.5 mJy. The model reproduced the available constraints at that time, but did not look at faint-enough galaxies to probe the existence of the flattening in the 1.1 mm number counts. The authors furthermore present the redshift distribution function for a survey at 1.1 mm with a flux density sensitivity of 1.5 mJy and find a median redshift of $z = 3$, with a quick drop at $z > 4$. This median redshift is higher than predicted by our model. The origin of this difference may lie in the adopted approach to estimate the dust mass of galaxies. Hayward et al. (2013b) adopt a fixed dust-to-metal ratio, a different mass–metallicity relation, and a different approach to estimate the gas mass of galaxies. As demonstrated in Appendix A of this paper (see Figure 7), these different approaches result in changes in the normalization of the number counts and small changes in their shape. Especially given the difference between the Zahid et al. (2013) and Maiolino et al. (2008) mass–metallicity relations, it is not surprising that this leads to a different redshift distribution.

Similar to the work presented in this paper, Hayward et al. (2013a) coupled the fitting functions from Hayward et al. (2011) to the subhalo abundance matching model presented in Behroozi et al. (2013a). Hayward et al. were particularly interested in the effects of blending (i.e., spatially and physically unassociated galaxies blending within one beam) on the derived 850 μm number counts of single-dish surveys and found that, indeed, for single-dish surveys, blending contributes significantly to the number counts at flux densities brighter than 2 mJy (the exact contribution of blending to the bright end of the number counts depends on the adopted beam size). In this work, we are mostly comparing our model predictions to observations that probe fainter regimes (fainter than 2 mJy at 850 μm), where blending is less of an issue and/or based on ALMA results, for which the beam size is sufficiently small to easily separate the individual sources.

Béthermin et al. (2017; see also Béthermin et al. 2012) developed a semiempirical model for the number counts of galaxies. This model is conceptually similar to the work presented here, but also accounts for the effect of lensing on the number counts of galaxies. The authors find a flattening in the 1.2 mm number counts at flux densities below 0.1 mJy, although not as strong as we find and suggested by observations. The authors furthermore explore the redshift distribution of galaxies, exploring a scenario with a survey depth of 4 mJy at 850 μm and 1.5 mJy at

1.2 mm (see also Béthermin et al. 2015). Béthermin et al. (2017) find that for the latter scenario, the redshift distribution peaks at around $z = 2$–3, slightly higher than our findings. The authors do not aim to explore what the properties are of the galaxies that contribute to the number counts at different flux densities.

Casey et al. (2018) also presented a model for the (among others) 1.1 mm and 850 μm number counts. Casey et al. explore a number of star formation history scenarios (especially focusing on the fraction of dust-obscured SF at $z > 4$) and investigate how these changes in the star formation histories manifest themselves in the (sub)millimeter number counts. The authors do not focus on flux densities faint enough to discuss their theoretical predictions for a flattening in the number counts.

5. Conclusions

In this paper, we presented a semiempirical model for the number counts of galaxies at 1.1 mm and 850 μm. This model is based upon the UniverseMachine (Behroozi et al. 2019; a model that predicts the stellar mass and SFR distribution of galaxies over cosmic time) with theoretical and empirical relations that predict the dust emission of galaxies as a function of their SFR and dust mass. This model can explain the observations at flux levels that were not reachable pre-ALMA. We summarize our main results below.

1. The predictions by our fiducial model are in good agreement with the observed cumulative number counts and number counts in bins of different galaxy properties. The model reproduces the flattening observed in the 1.1 mm number counts of recent deep surveys with ALMA. A similar flattening is predicted for the 850 μm number counts below 1 mJy.
2. We demonstrate that the flattening in the 1.1 mm number counts reflects the shape of the underlying galaxy population at $z = 1$–2, i.e., the observations are probing the knee and the shallow faint-end slope of the 1.1 mm luminosity function.
3. The galaxies at the "knee" of the 1.1 mm number counts have redshifts between $z = 1$ and $z = 2$, stellar masses around $5 \times 10^{10} M_{\odot}$, and dust masses of the order $10^8\ M_{\odot}$.
4. The observed ASPECS redshift distribution of 1.1 mm ALMA detections is in agreement with the model predictions after we account for field-to-field variance.
5. Future dust continuum surveys at 1.1 mm and 850 μm that aim to detect large numbers of sources through their dust emission should cover large areas on the sky once below a flux density of $\sim$0.1 mJy (at 1.1 mm, $\sim$0.3 mJy at 850 μm), rather than integrating to faint flux densities over small portions on the sky.
6. Our model successfully reproduces the number counts of galaxies without the need to adopt an IMF different from Chabrier (2003). This is in contrast with theoretical models suggesting that a top-heavy IMF is responsible for the observed number counts of bright millimeter galaxies.
7. The success of our model in reproducing the number counts of galaxies suggests that the adopted empirical relations in our fiducial model (to estimate the gas mass, the gas-phase metallicity, obscured fraction of star formation, dust mass, and dust continuum flux of galaxies) are valid up to $z = 2$. Different choices for the empirical relations lead to poorer agreement with the observations.

The success of our model to describe the number counts of galaxies at 1.1 mm and which galaxies are responsible for these number counts also means that we have exhausted the amount of information about galaxy physics that can be extracted from dust continuum number counts, mainly because the number counts are biased toward a narrow redshift range from redshift one to two. To further our knowledge about galaxy physics from continuum observations, future observational efforts should focus on the dust continuum properties in discrete redshift bins (e.g., dust continuum luminosity function), as a function of other galaxy properties, and on spatially resolved, multiband dust continuum properties of galaxies and their connection to the resolved stellar and gas properties of galaxies.

We thank Caitlin Casey, Philipp Lang, Desika Narayanan, and I-Ting Ho for useful discussions, and Claudia Lagos and especially Ian Smail for comments on an earlier version of this paper. We additionally thank the referee for constructive comments. Computations for this work were performed on Rusty at the Center for Computational Astrophysics, Flatiron Institute. The Flatiron Institute is supported by the Simons Foundation. F.W. acknowledges support from ERC Advanced Grant 740246 (Cosmic Gas). Este trabajo contó con el apoyo de CONICYT + Programa de Astronomía+ Fondo CHINA-CONICYT CAS16026. Este trabajo cont ó con el apoyo de CONICYT + PCI + INSTITUTO MAX PLANCK DE ASTRONOMIA MPG190030. R.J.A. was supported by FONDECYT grant No. 1191124. F.E.B. acknowledges support from CONICYT-Chile (Basal AFB-170002, FONDO ALMA 31160033, FONDECYT Regular 1190818), the Ministry of Economy, Development, and Tourism's Millennium Science Initiative through grant IC120009, awarded to The Millennium Institute of Astrophysics, MAS. D.R. acknowledges support from the National Science Foundation under grant No. AST-1614213 and from the Alexander von Humboldt Foundation through a Humboldt Research Fellowship for Experienced Researchers. This paper makes use of the ALMA data ADS/JAO.ALMA#2016.1.00324.L. ALMA is a partnership of ESO (representing its member states), NSF (USA) and NINS (Japan), together with NRC (Canada), NSC and ASIAA (Taiwan), and KASI (Republic of Korea), in cooperation with the Republic of Chile. The Joint ALMA Observatory is operated by ESO, AUI/NRAO, and NAOJ. The National Radio Astronomy Observatory is a facility of the National Science Foundation operated under cooperative agreement by Associated Universities, Inc.

Appendix A
Is the Flattening in the Number Counts Robust Against the Assumptions Made in the Semiempirical Model

In the main body of this paper, we have connected the predictions from the UniverseMachine to a number of empirical relations to estimate the submillimeter flux density of galaxies. In this appendix, we explore how robust our results are against the exact choice in these empirical relations. We replace the empirical relations in our fiducial model by other relations/assumptions proposed in the literature and show the resulting predicted number counts in Figure 7.

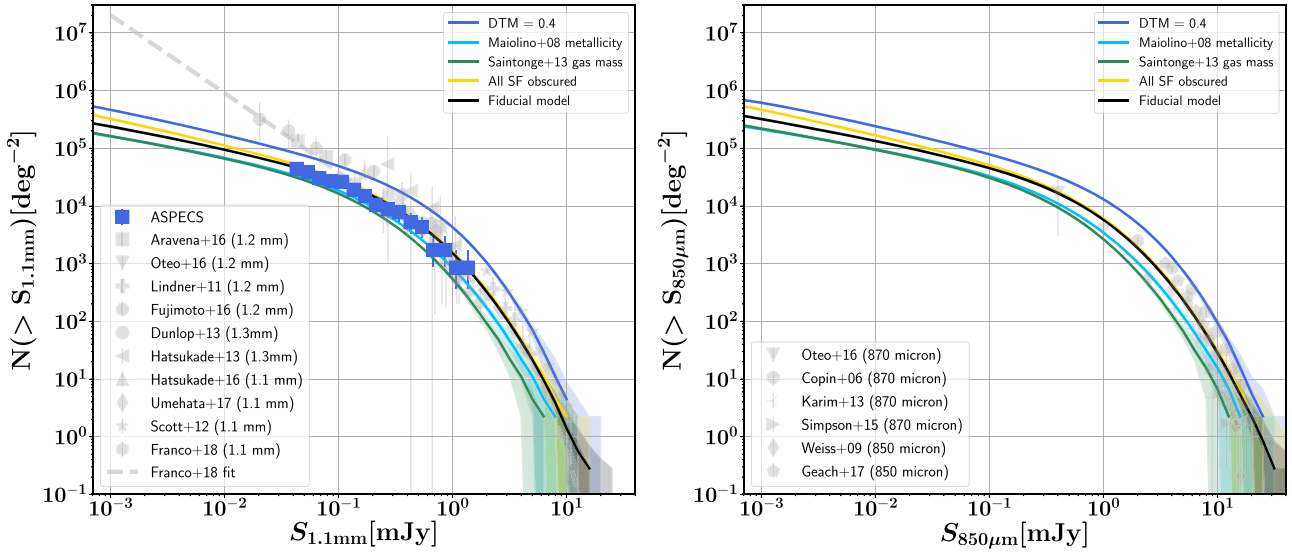

Figure 7. The observed and predicted 1.1 mm and 850 μm galaxy number counts. The black solid line marks the fiducial model discussed in this paper. The colored lines mark the number counts when replacing individual components of the model by different empirical relations/assumptions discussed in Appendix A. The shaded region marks the 1σ variance of the 100 random realizations when sampling over the error of the individual components of the model. There are some changes in the normalization of the number counts when varying individual components of the model within a factor of <2, but overall the shape of the number counts is robust against the changes applied to the model.

*Gas masses estimated following Saintonge et al. (*2013*)*—We have adopted the methodology presented in Popping et al. (2015a) to estimate the gas mass (atomic plus molecular) of galaxies. An alternative option is the fit for the H_2 mass of galaxies as a function of stellar mass, SFR, and redshift given in Saintonge et al. (2013; note that this prescription does not include a contribution by H I to the total gas mass). We find that the number counts are systematically a factor of 1.5–2 below the predictions of our fiducial model.

Fixed dust-to-metal ratio of 0.4—Theoretical models typically make the assumption that the dust-to-metal ratio of the ISM equals 0.4. When adopting the same value (thus not scaling the dust-to-metal ratio of the ISM as a function of the gas-phase metallicity), the predicted number counts are a factor of 1.5–2 above the predictions by our fiducial model. Although the overall normalization of the number counts changes, the flattening does not disappear.

Mass–metallicity relation from Maiolino et al. (2008)—An alternative fit of the gas-phase metallicity of galaxies as a function of their stellar mass and redshift in the redshift range from $z = 0$ to $z = 3.5$ was presented in Maiolino et al. (2008). We adopted the Zahid et al. (2013) relation for our fiducial model as this is based on a more robust sample of galaxies with a coherent metallicity calibration. The number counts predicted when adopting the Maiolino et al. (2008) mass–metallicity relation are a factor of $\sim$1.5 below the predictions by our fiducial model.

All star formation is obscured—We adopted the fit presented in Whitaker et al. (2017) to estimate the obscured fraction of SF. An extreme alternative is to assume that all SF happens in dust environments and $f_{\rm obscured} = 1$. We find that the resulting number counts are essentially the same as predicted by our fiducial model, expect for the faintest flux densities.

Summarizing, we find that the exact choice for the individual components of our model changes the normalization of the number counts, but not the presence of a flattening. This confirms that the flattening seen in the data is indeed a result of the underlying galaxy population and not due to the adopted approach to assign submillimeter luminosities to galaxies.

Appendix B
A Hypothetical Survey

In Figures 8 and 9, we show the predicted number of observed galaxies and their redshift distribution, respectively, by hypothetical future surveys (with ALMA). These are discussed in detail in Section 4.1

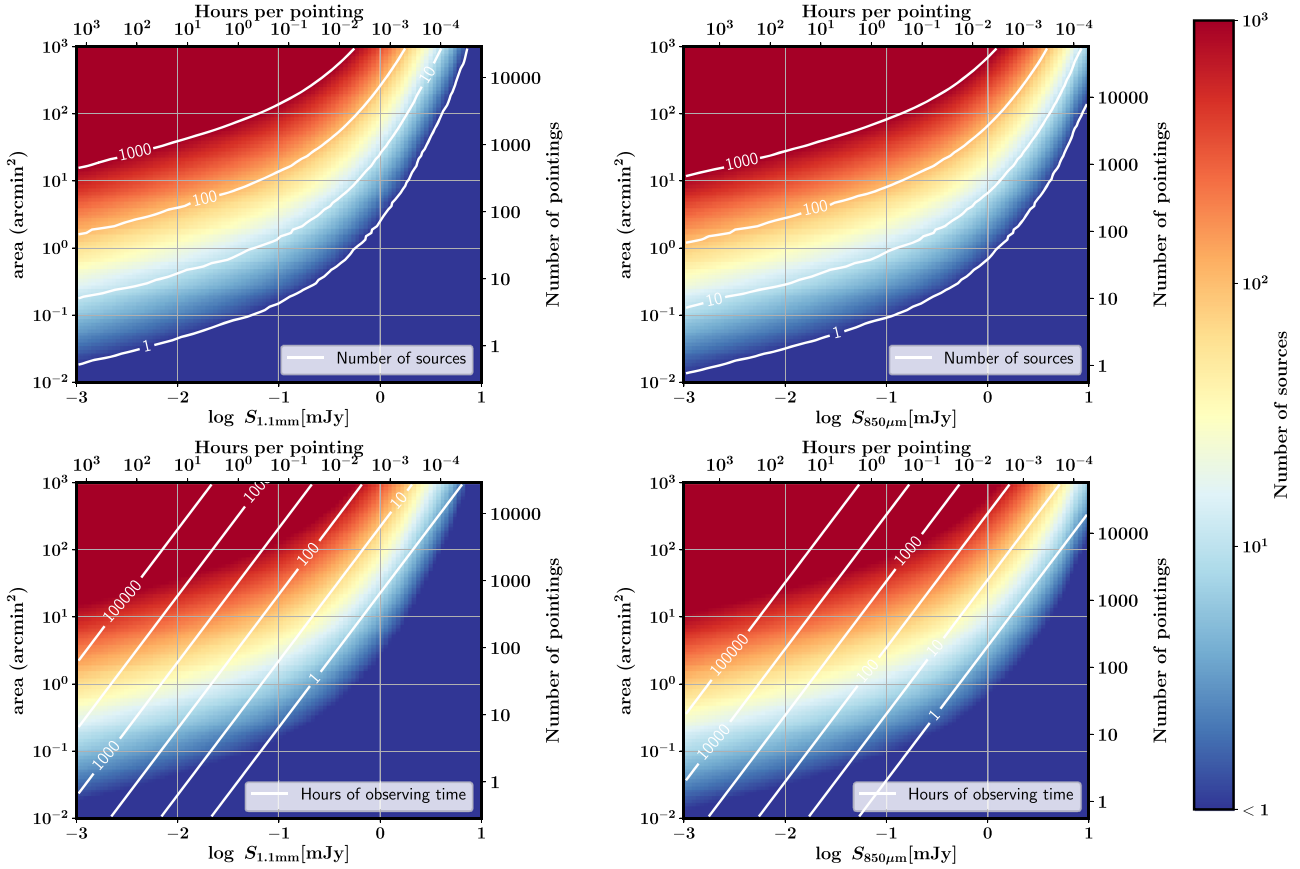

Figure 8. The expected number of sources for a hypothetical survey at 1.1 mm (left column) and 850 μm (right column), as a function of the survey depth and covered area, as well as the number of hours per pointing it takes to reach this depth (at a signal-to-noise ratio of 3) and the number of pointings necessary to cover the area assuming Nyquist sampling (all assuming standard ALMA assumptions for 50 antennas). In the top row, contours depict lines of a fixed number of expected sources. In the bottom row, contours depict a fixed total on-source observing time. Below flux densities of 0.1 (0.3 mJy), a wide survey at 1.1 mm (850 μm) is more (cost) efficient to increase the number of detected sources than a deep pointed survey.

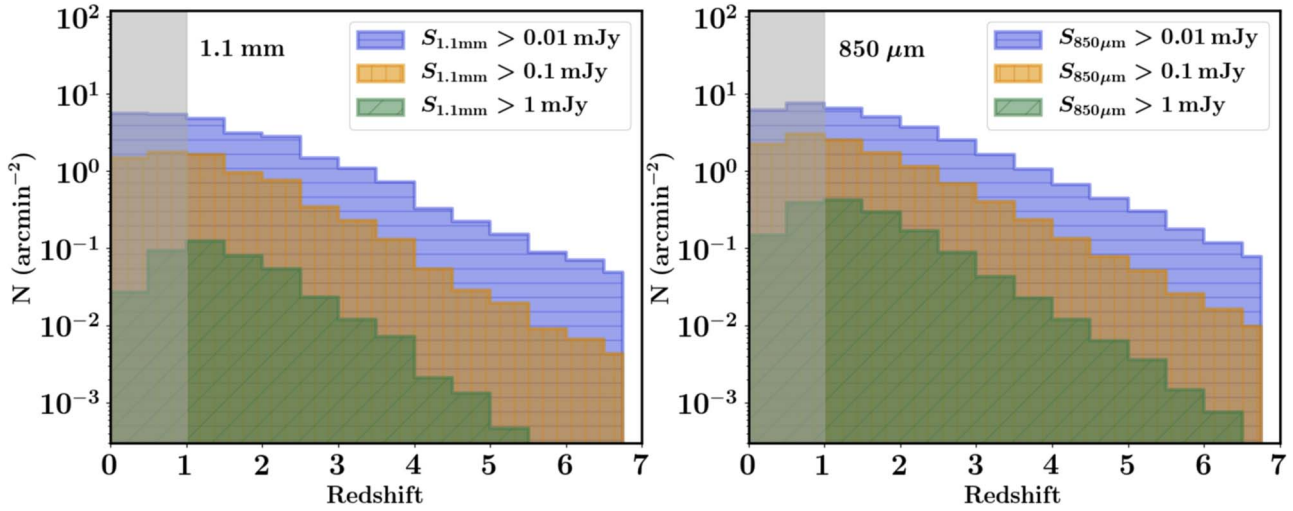

Figure 9. The redshift distribution of galaxies as a function of their 1.1 mm (left) and 850 μm (right) flux density. A different survey depth results in preferentially detecting galaxies at different redshifts. To efficiently detect galaxies, a shallow but wide survey is more time efficient that a narrow but deeper survey. The gray shaded area (at $z < 1$) marks the regime where the model predictions cannot be fully trusted because the negative k-correction no longer applies at those redshifts.

ORCID iDs

Gergö Popping https://orcid.org/0000-0003-1151-4659
Fabian Walter https://orcid.org/0000-0003-4793-7880
Jorge González-López https://orcid.org/0000-0003-3926-1411
Christopher C. Hayward https://orcid.org/0000-0003-4073-3236
Paul van der Werf https://orcid.org/0000-0001-5434-5942
Manuel Aravena https://orcid.org/0000-0002-6290-3198

Roberto J. Assef https://orcid.org/0000-0002-9508-3667
Leindert Boogaard https://orcid.org/0000-0002-3952-8588
Franz E. Bauer https://orcid.org/0000-0002-8686-8737
Paulo C. Cortes https://orcid.org/0000-0002-3583-780X
Tanio Díaz-Santos https://orcid.org/0000-0003-0699-6083
Roberto Decarli https://orcid.org/0000-0002-2662-8803
Rob Ivison https://orcid.org/0000-0001-5118-1313
Dominik Riechers https://orcid.org/0000-0001-9585-1462
Hans-Walter Rix https://orcid.org/0000-0003-4996-9069
Axel Weiss https://orcid.org/0000-0003-4678-3939

References

Aravena, M., Decarli, R., Gónzalez-López, J., et al. 2019, ApJ, 882, 136
Aravena, M., Decarli, R., Walter, F., et al. 2016, ApJ, 833, 68
Baugh, C. M., Lacey, C. G., Frenk, C. S., et al. 2005, MNRAS, 356, 1191
Behroozi, P., Wechsler, R. H., Hearin, A. P., & Conroy, C. 2019, MNRAS, 488, 3143
Behroozi, P. S., Wechsler, R. H., & Conroy, C. 2013a, ApJ, 770, 57
Behroozi, P. S., Wechsler, R. H., & Wu, H.-Y. 2013b, ApJ, 762, 109
Behroozi, P. S., Wechsler, R. H., Wu, H.-Y., et al. 2013c, ApJ, 763, 18
Béthermin, M., Daddi, E., Magdis, G., et al. 2012, ApJL, 757, L23
Béthermin, M., De Breuck, C., Sargent, M., & Daddi, E. 2015, A&A, 576, L9
Béthermin, M., Wu, H.-Y., Lagache, G., et al. 2017, A&A, 607, A89
Bigiel, F., Leroy, A., Walter, F., et al. 2008, AJ, 136, 2846
Blitz, L., & Rosolowsky, E. 2006, ApJ, 650, 933
Boogaard, L. A., Decarli, R., González-López, J., et al. 2019, ApJ, 882, 140
Bouwens, R. J., Aravena, M., Decarli, R., et al. 2016, ApJ, 833, 72
Carniani, S., Maiolino, R., De Zotti, G., et al. 2015, A&A, 584, A78
Casey, C. M., Narayanan, D., & Cooray, A. 2014, PhR, 541, 45
Casey, C. M., Zavala, J. A., Spilker, J., et al. 2018, ApJ, 862, 77
Chabrier, G. 2003, PASP, 115, 763
Coppin, K., Chapin, E. L., Mortier, A. M. J., et al. 2006, MNRAS, 372, 1621
Cowley, W. I., Béthermin, M., Lagos, C. d. P., et al. 2017, MNRAS, 467, 1231
Cowley, W. I., Lacey, C. G., Baugh, C. M., & Cole, S. 2015, MNRAS, 446, 1784
da Cunha, E., Groves, B., Walter, F., et al. 2013, ApJ, 766, 13
Davé, R., Anglés-Alcázar, D., Narayanan, D., et al. 2019, MNRAS, 486, 2827
De Vis, P., Jones, A., Viaene, S., et al. 2019, A&A, 623, A5
Decarli, R., Walter, F., Gónzalez-López, J., et al. 2019, ApJ, 882, 138
Draine, B. T. 2011, Physics of the Interstellar and Intergalactic Medium (Princeton, NJ: Princeton Univ. Press)
Dunlop, J. S., McLure, R. J., Biggs, A. D., et al. 2017, MNRAS, 466, 861
Eales, S., Lilly, S., Webb, T., et al. 2000, AJ, 120, 2244
Feldmann, R. 2015, MNRAS, 449, 3274
Fixsen, D. J., Dwek, E., Mather, J. C., Bennett, C. L., & Shafer, R. A. 1998, ApJ, 508, 123
Fontanot, F., Somerville, R. S., Silva, L., Monaco, P., & Skibba, R. 2009, MNRAS, 392, 553
Franco, M., Elbaz, D., Béthermin, M., et al. 2018, A&A, 620, A152
Fujimoto, S., Ouchi, M., Ono, Y., et al. 2016, ApJS, 222, 1
Geach, J. E., Dunlop, J. S., Halpern, M., et al. 2017, MNRAS, 465, 1789
González-López, J., Decarli, R., Pavesi, R., et al. 2019, ApJ, 882, 139
González-López, J., Decarli, R., Walter, F., et al. 2020, arXiv:2002.07199
Granato, G. L., Lacey, C. G., Silva, L., et al. 2000, ApJ, 542, 710
Hatsukade, B., Kohno, K., Umehata, H., et al. 2016, PASJ, 68, 36
Hatsukade, B., Ohta, K., Seko, A., Yabe, K., & Akiyama, M. 2013, ApJL, 769, L27
Hayward, C. C., Behroozi, P. S., Somerville, R. S., et al. 2013a, MNRAS, 434, 2572
Hayward, C. C., Kereš, D., Jonsson, P., et al. 2011, ApJ, 743, 159
Hayward, C. C., Narayanan, D., Kereš, D., et al. 2013b, MNRAS, 428, 2529
Hou, K.-C., Aoyama, S., Hirashita, H., Nagamine, K., & Shimizu, I. 2019, MNRAS, 485, 1727
Imara, N., Loeb, A., Johnson, B. D., Conroy, C., & Behroozi, P. 2018, ApJ, 854, 36
Inami, H., Bacon, R., Brinchmann, J., et al. 2017, A&A, 608, A2
Jonsson, P. 2006, MNRAS, 372, 2
Karim, A., Swinbank, A. M., Hodge, J. A., et al. 2013, MNRAS, 432, 2
Kewley, L. J., & Ellison, S. L. 2008, ApJ, 681, 1183
Klypin, A., Yepes, G., Gottlöber, S., Prada, F., & Heß, S. 2016, MNRAS, 457, 4340
Knudsen, K. K., van der Werf, P. P., & Kneib, J.-P. 2008, MNRAS, 384, 1611
Lacey, C. G., Baugh, C. M., Frenk, C. S., et al. 2016, MNRAS, 462, 3854
Lagos, C. d. P., Robotham, A. S. G., Trayford, J. W., et al. 2019, MNRAS, 489, 4196
Leja, J., Johnson, B. D., Conroy, C., et al. 2019, ApJ, 877, 140
Lindner, R. R., Baker, A. J., Omont, A., et al. 2011, ApJ, 737, 83
Lu, Y., Mo, H. J., Weinberg, M. D., & Katz, N. 2011, MNRAS, 416, 1949
Lu, Y., Wechsler, R. H., Somerville, R. S., et al. 2014, ApJ, 795, 123
Madau, P., & Dickinson, M. 2014, ARA&A, 52, 415
Magdis, G. E., Daddi, E., Béthermin, M., et al. 2012, ApJ, 760, 6
Magnelli, B., Boogaard, L., Decarli, R., et al. 2020, arXiv:2002.08640
Maiolino, R., Nagao, T., Grazian, A., et al. 2008, A&A, 488, 463
McKinnon, R., Torrey, P., Vogelsberger, M., Hayward, C. C., & Marinacci, F. 2017, MNRAS, 468, 1505
Miettinen, O., Delvecchio, I., Smolčić, V., et al. 2017, A&A, 606, A17
Moster, B. P., Somerville, R. S., Newman, J. A., & Rix, H.-W. 2011, ApJ, 731, 113
Motte, F., Nony, T., Louvet, F., et al. 2018, NatAs, 2, 478
Muñoz Arancibia, A. M., González-López, J., Ibar, E., et al. 2018, A&A, 620, A125
Narayanan, D., Davé, R., Johnson, B. D., et al. 2018, MNRAS, 474, 1718
Ono, Y., Ouchi, M., Kurono, Y., & Momose, R. 2014, ApJ, 795, 5
Oteo, I., Zwaan, M. A., Ivison, R. J., Smail, I., & Biggs, A. D. 2016, ApJ, 822, 36
Planck Collaboration, Aghanim, N., Akrami, Y., et al. 2018, arXiv:1807.06209
Popping, G., Behroozi, P. S., & Peeples, M. S. 2015a, MNRAS, 449, 477
Popping, G., Caputi, K. I., Trager, S. C., et al. 2015b, MNRAS, 454, 2258
Popping, G., Pillepich, A., Somerville, R. S., et al. 2019, ApJ, 882, 137
Popping, G., Somerville, R. S., & Galametz, M. 2017, MNRAS, 471, 3152
Pozzi, F., Calura, F., Zamorani, G., et al. 2020, MNRAS, 491, 5073
Puget, J.-L., Abergel, A., Bernard, J.-P., et al. 1996, A&A, 308, L5
Rodríguez-Puebla, A., Behroozi, P., Primack, J., et al. 2016, MNRAS, 462, 893
Romano, D., Matteucci, F., Zhang, Z. Y., Papadopoulos, P. P., & Ivison, R. J. 2017, MNRAS, 470, 401
Safarzadeh, M., Lu, Y., & Hayward, C. C. 2017, MNRAS, 472, 2462
Saintonge, A., Lutz, D., Genzel, R., et al. 2013, ApJ, 778, 2
Schneider, F. R. N., Sana, H., Evans, C. J., et al. 2018, Sci, 359, 69
Schreiber, C., Elbaz, D., Pannella, M., et al. 2018, A&A, 609, A30
Scott, K. S., Wilson, G. W., Aretxaga, I., et al. 2012, MNRAS, 423, 575
Scoville, N., Sheth, K., Aussel, H., et al. 2016, ApJ, 820, 83
Simpson, J. M., Smail, I., Swinbank, A. M., et al. 2015, ApJ, 807, 128
Smail, I., Ivison, R. J., Blain, A. W., & Kneib, J.-P. 2002, MNRAS, 331, 495
Somerville, R. S., Gilmore, R. C., Primack, J. R., & Domínguez, A. 2012, MNRAS, 423, 1992
Somerville, R. S., Hopkins, P. F., Cox, T. J., Robertson, B. E., & Hernquist, L. 2008, MNRAS, 391, 481
Speagle, J. S., Steinhardt, C. L., Capak, P. L., & Silverman, J. D. 2014, ApJS, 214, 15
Tomczak, A. R., Quadri, R. F., Tran, K.-V. H., et al. 2014, ApJ, 783, 85
Umehata, H., Tamura, Y., Kohno, K., et al. 2017, ApJ, 835, 98
van der Wel, A., Franx, M., van Dokkum, P. G., et al. 2014, ApJ, 788, 28
Walter, F., Decarli, R., Aravena, M., et al. 2016, ApJ, 833, 67
Weiss, A., Kovács, A., Coppin, K., et al. 2009, ApJ, 707, 1201
Whitaker, K. E., Pope, A., Cybulski, R., et al. 2017, ApJ, 850, 208
Zahid, H. J., Dima, G. I., Kudritzki, R.-P., et al. 2014, ApJ, 791, 130
Zahid, H. J., Geller, M. J., Kewley, L. J., et al. 2013, ApJL, 771, L19
Zhang, Z.-Y., Romano, D., Ivison, R. J., Papadopoulos, P. P., & Matteucci, F. 2018, Natur, 558, 260